Mesoscale Air-Sea Interaction and Eddy Potential Energy Budget
Is It Important?

Yiming Guo & Stuart P. Bishop (NC State)
Frank O. Bryan & Scott D. Bachman (NCAR)

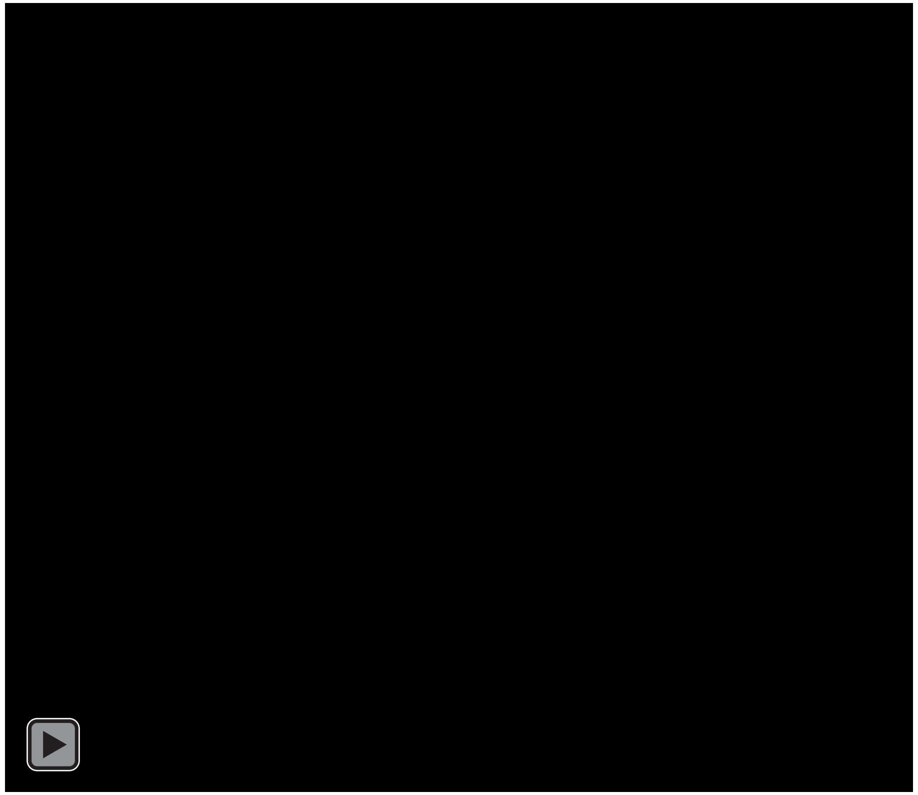

Surface $\overline{v'\theta'}$ from 1/10° POP

Ocean Model Working Group – February 4, 2021

Ocean mesoscale

- Dominant reservoir of kinetic energy.

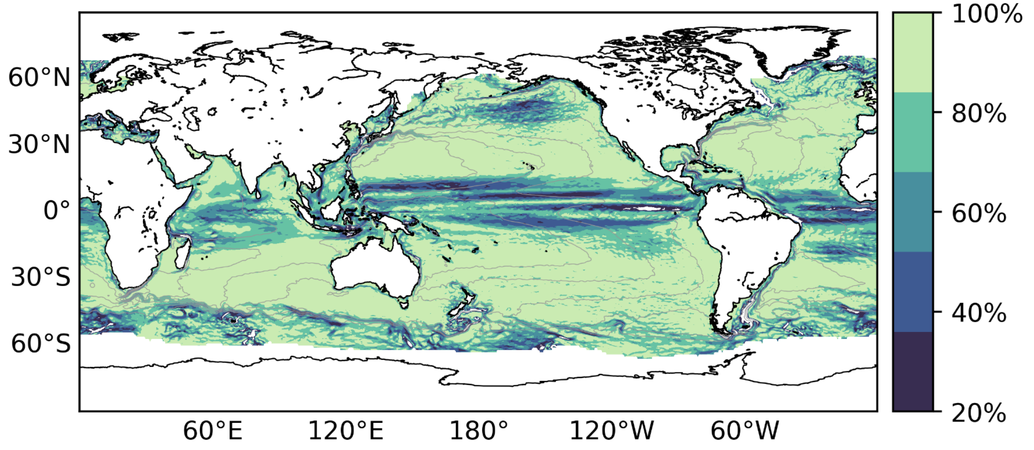

[Surface ratio of EKE and TKE]

- Essential to nutrient redistribution.

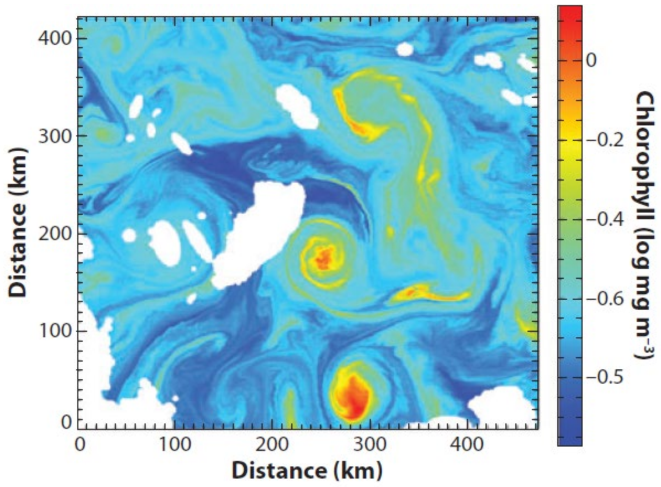

(Klein and Lapeyre 2009)

- Modulate poleward heat transport.

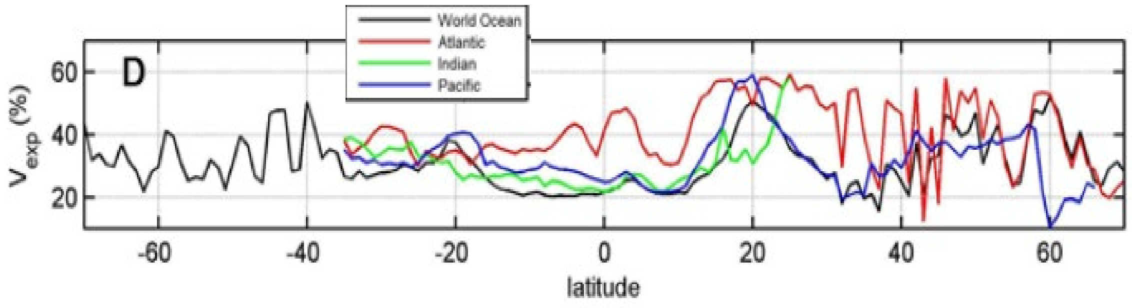

(Volkov et al. 2008)

- Impact on atmospheric conditions.

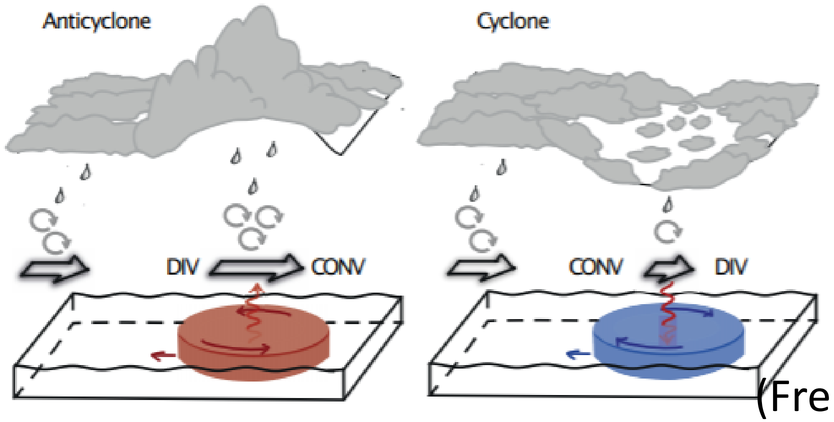

(Frenger et al. 2013)

The flow of energy

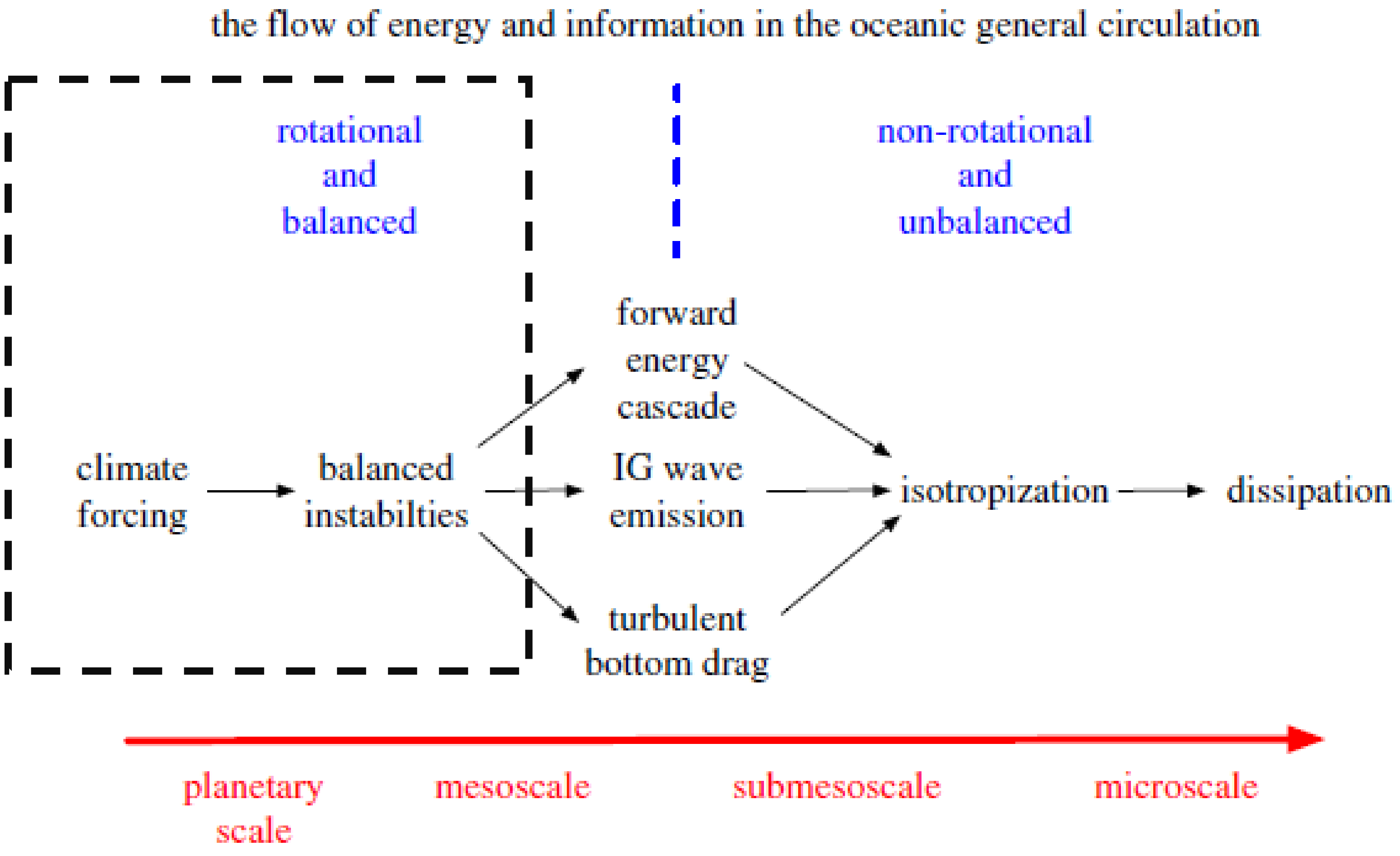

(McWilliams 2016)

Adiabatic Eddy Potential Energy Budget

Assumptions: Steady state; No advection by eddy velocity; No diabatic forcing.

‘EPE’ equation: $\bar{\boldsymbol{v}} \cdot \nabla \frac{\overline{T'^2}}{2} + \overline{\boldsymbol{v}'T'} \cdot \nabla \bar{T} + \overline{w'T'} \frac{\partial \bar{T}}{\partial z} = 0$ (Marshall and Shutts 1981)

$$\overline{\boldsymbol{v}'T'} = \overline{\boldsymbol{v}'T'}^{rot} + \overline{\boldsymbol{v}'T'}^{div}$$

$$\bar{\boldsymbol{v}} \cdot \nabla \frac{\overline{T'^2}}{2} + \overline{\boldsymbol{v}'T'}^{rot} \cdot \nabla \bar{T} = 0$$

$$-\overline{\boldsymbol{v}'T'}^{div} \cdot \nabla \bar{T} - \overline{w'T'} \frac{\partial \bar{T}}{\partial z} = 0$$

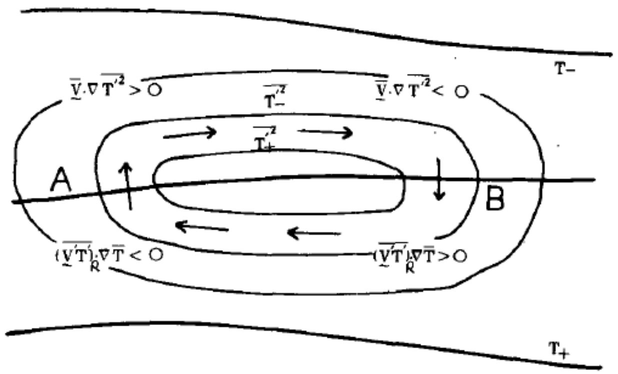

FIG. 1. Schematic picture showing rotational heat fluxes (arrows) in relation to the mean temperature (open contours) and the eddy potential energy (closed contours). Eddies generated

(Marshall and Shutts 1981)

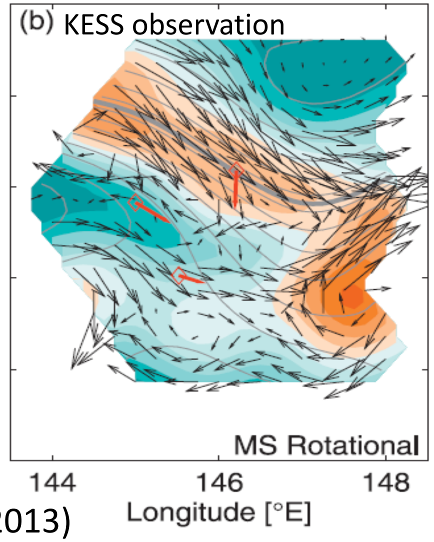

(Bishop et al. 2013)

MPE → Baroclinic Conversion (BC) → EPE → Potential-Kinetic Conversion (PKC) → EKE

Divergent and rotational eddy heat flux

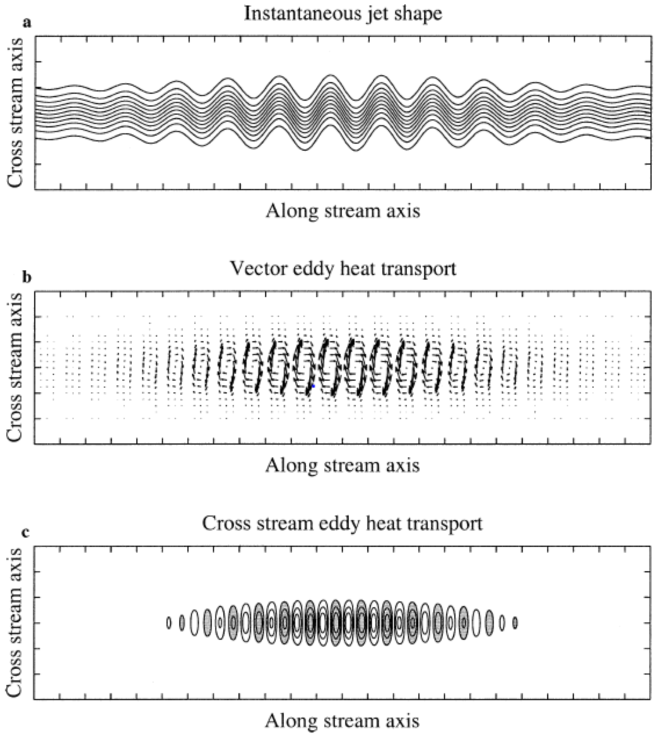

(Jayne and Marotzke, 2002)

The eddy heat flux can be rewritten into a rotational part and a divergent part as Helmholtz decomposition:

$$\overline{\vec{v}'T'} = \underbrace{k \times \nabla\psi}_{\overline{\vec{v}'T'}_{rot}} + \underbrace{\nabla\phi}_{\overline{\vec{v}'T'}_{div}} \ , \qquad (1)$$

Which satisfies

$$\nabla \cdot \overline{\vec{v}'T'}_{rot} = \nabla \times \overline{\vec{v}'T'}_{div} = 0 \, , \qquad (2)$$

A 2D Poisson equation appears after taking the divergence of equation (1):

$$\nabla \cdot \left(\overline{\vec{v}'T'}\right) = \nabla^2\phi, \qquad (3)$$

- Eddy energy is dominated by the meandering states of the zonal jets.
- The divergent component of the eddy heat flux is the dynamically important flux. (Marshall and Shutts, 1981)

Divergent and rotational eddy heat flux

Reconstruction on the mixed-layer eddy heat flux based on observations

$$Q_{ML} = \rho_0 c_p \overline{v'T'} H$$

- **Sea surface height (SSH) and geostrophic velocity.**

From Copernicus Marine and Environment Monitoring Services (CMEMS). Daily data from 1993 to present. Horizontal resolution is $0.25°$.

- **Sea surface temperature (SST).**

From NOAA OISST version2. Daily data from 1981 to present. Horizontal resolution is $0.25°$.

- **Mixed layer Climatology**

From the Monthly Isopycnal & Mixed-layer Ocean Climatology (MIMOC). Horizontal resolution is $0.5°$.

Divergent and rotational eddy heat flux

$$Q_{ML} = \rho_0 c_p \overline{v'T'} H$$

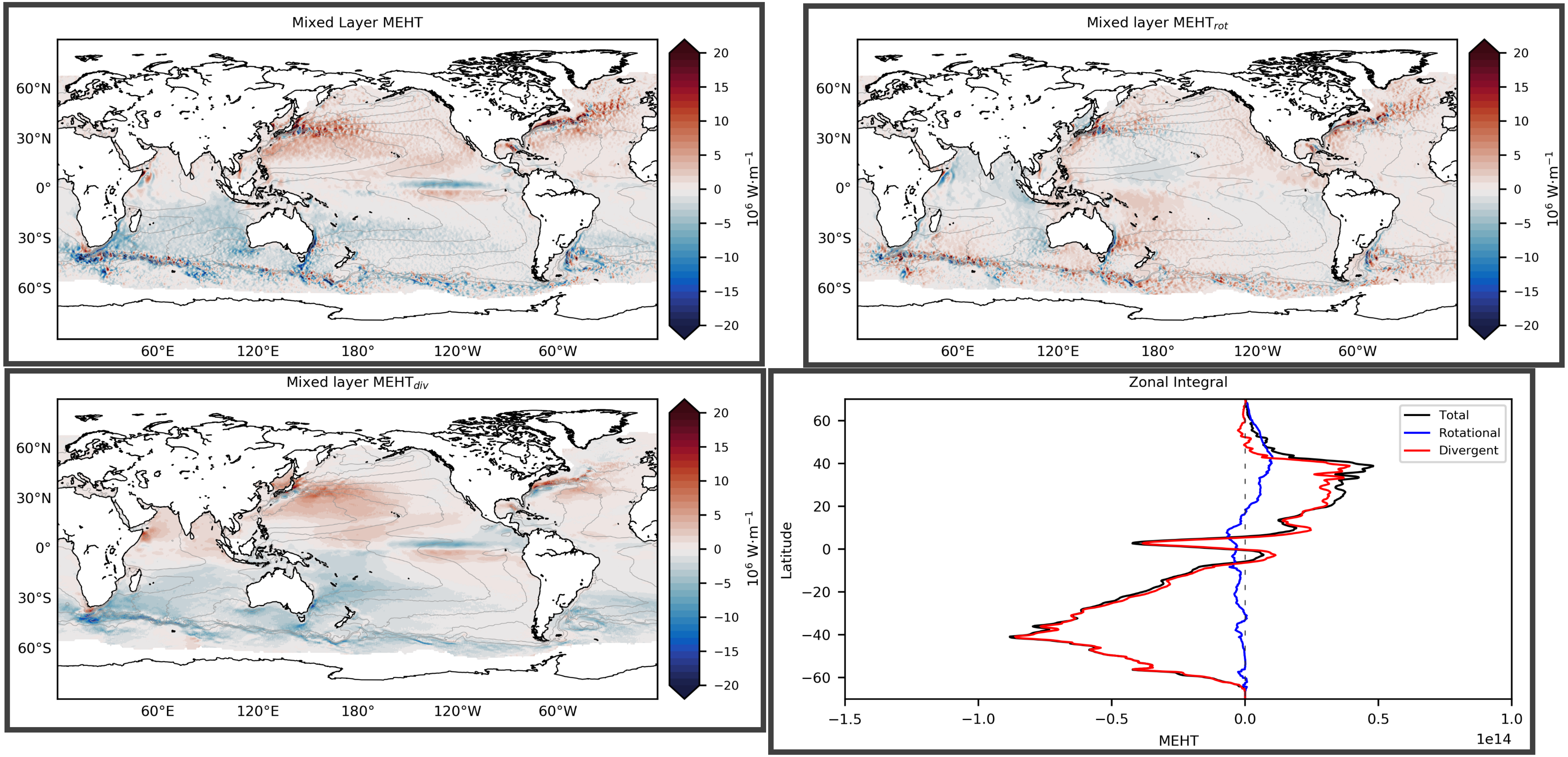

Based on satellite observed SSH and SST; MIMOC ML climatology

Divergent and rotational eddy heat flux

$-\overline{\boldsymbol{v}'T'}^{rot} \cdot \nabla\bar{T}$

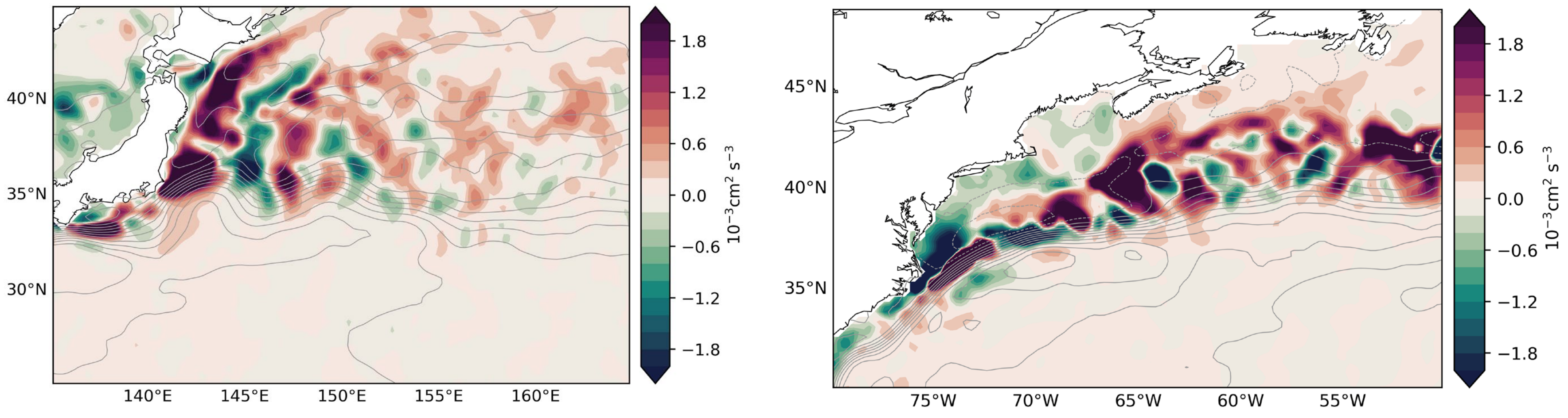

$-\overline{\boldsymbol{v}'T'}^{div} \cdot \nabla\bar{T}$

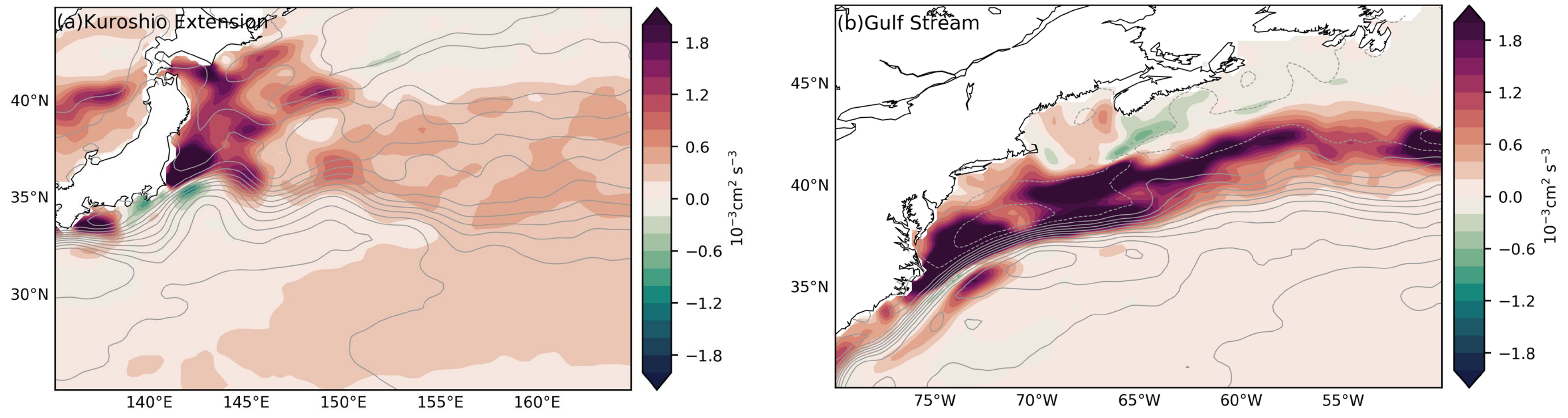

- Positive and negative conversions occur alternatively along the major currents, which obscure the actual down-gradient fluxes.
- The decomposition is necessary for **regional** energetic analysis.

Adiabatic Eddy Potential Energy Budget

Steady state adiabatic EPE balance (Marshall and Shutts 1981)

$$-\overline{\boldsymbol{v}'T'}^{div} \cdot \nabla\bar{T} - \overline{w'T'}\frac{\partial \bar{T}}{\partial z} = 0$$

- ➢ **JRA55 forced POP simulation.**

Nominal 0.1°; 62 levels; 5-day output; Year 1999-2018;

- Strong spatial coherence between downgradient horizontal and upgradient vertical eddy heat fluxes.

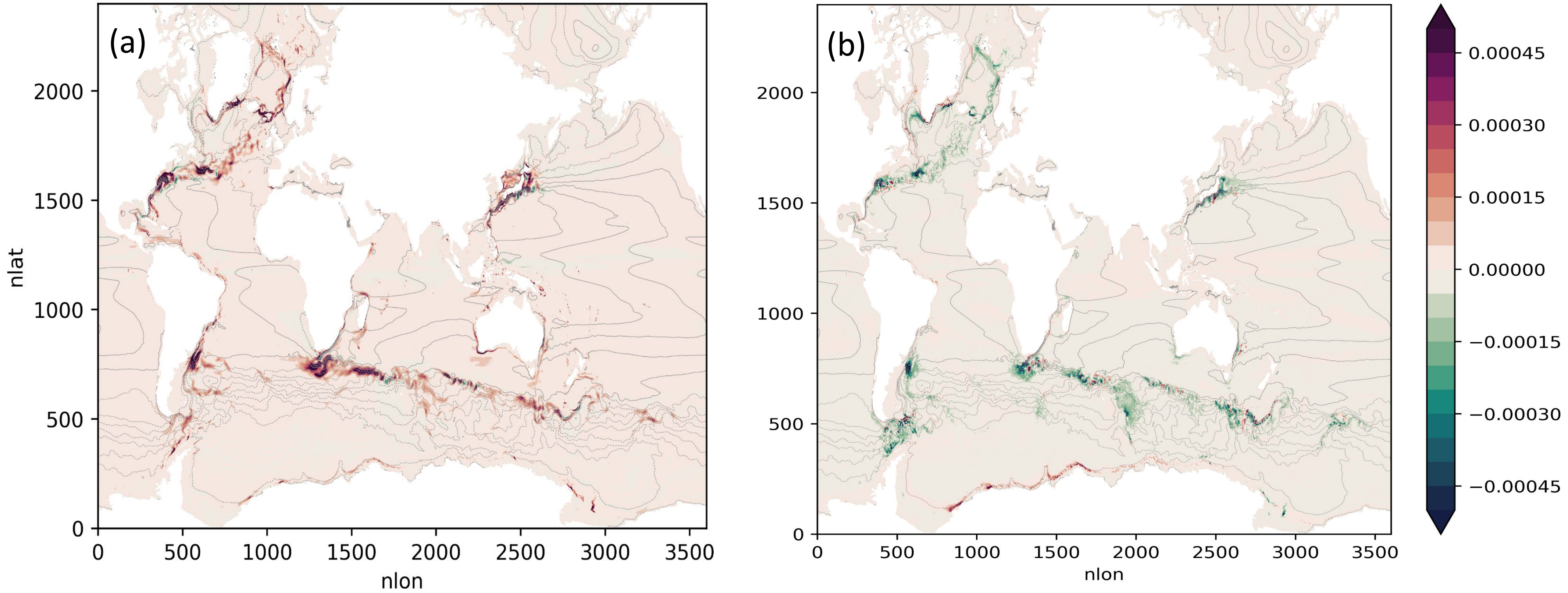

Depth-integrated (a) Divergent BC rate and (b) PKC rate in the POP model (unit: $°\mathrm{C}^2\ m \cdot s^{-1}$).

Adiabatic Eddy Potential Energy Budget

Steady state adiabatic EPE balance (Marshall and Shutts 1981)

$$-\overline{\boldsymbol{v}'T'}^{div} \cdot \nabla\bar{T} - \overline{w'T'}\frac{\partial \bar{T}}{\partial z} = 0$$

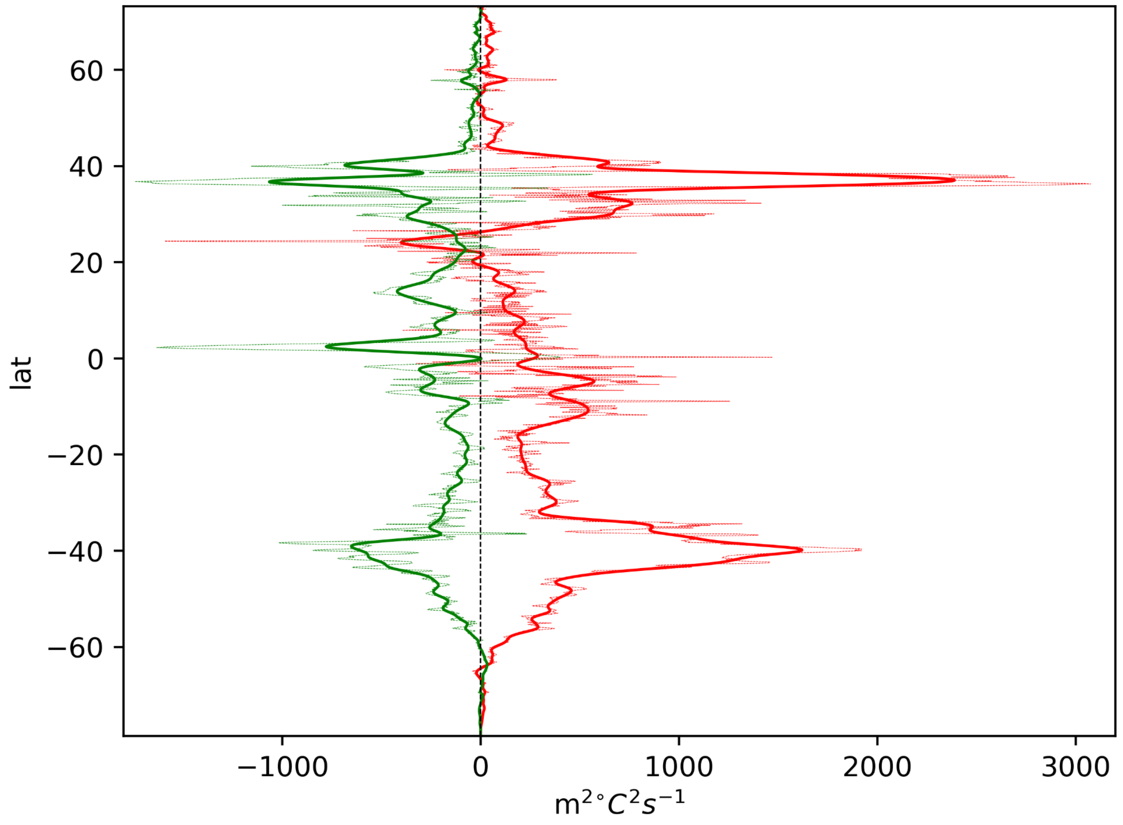

From 1/10° POP model

- Strong spatial coherence between downgradient horizontal and upgradient vertical eddy heat fluxes.
- o(MPE−EPE) > o(EPE−EKE)

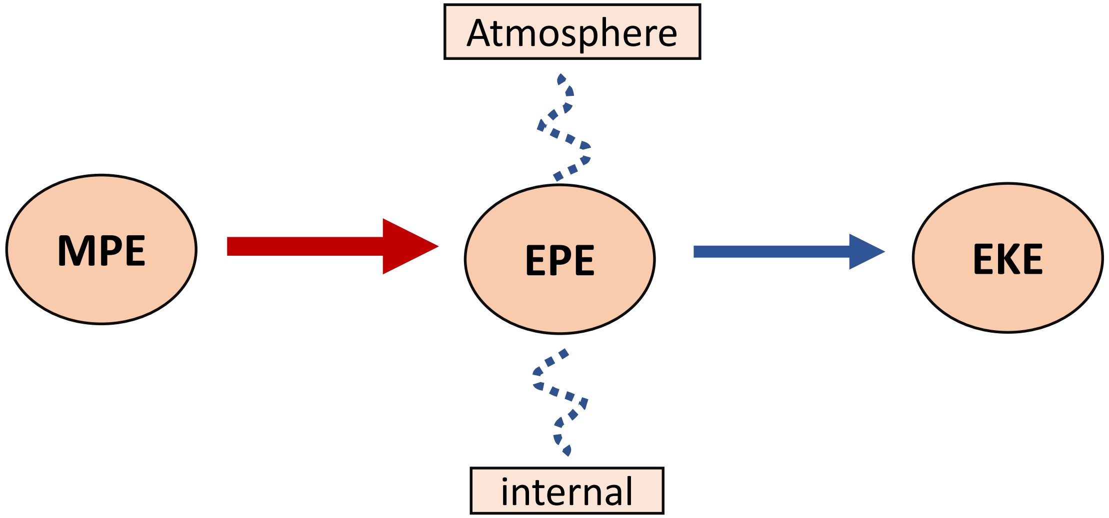

Diabatic Eddy Potential Energy Budget

Full EPE equation (from thermal contribution):

$$\frac{\partial \overline{\frac{T'^2}{2}}}{\partial t} = -(\overline{\boldsymbol{v}}+\boldsymbol{v}')\cdot\nabla\overline{\frac{T'^2}{2}} - \overline{\boldsymbol{v}'T'}\cdot\nabla_h\overline{T} - \overline{w'T'}\frac{\partial\overline{T}}{\partial z} + T'\frac{\partial}{\partial z}\left(\frac{Q'}{\rho_o C_p} + \kappa\frac{\partial T}{\partial z}\right) + T'\cdot A_h\nabla^2 T$$

- Tendency
- Mean+eddy advection
- BC ($BC^{rot}+BC^{div}$)
- PKC
- Vertical mixing
- Horizontal diffusion

$$\frac{\alpha^2 g^2}{C_p {N_r}^2}\overline{T'Q'}$$

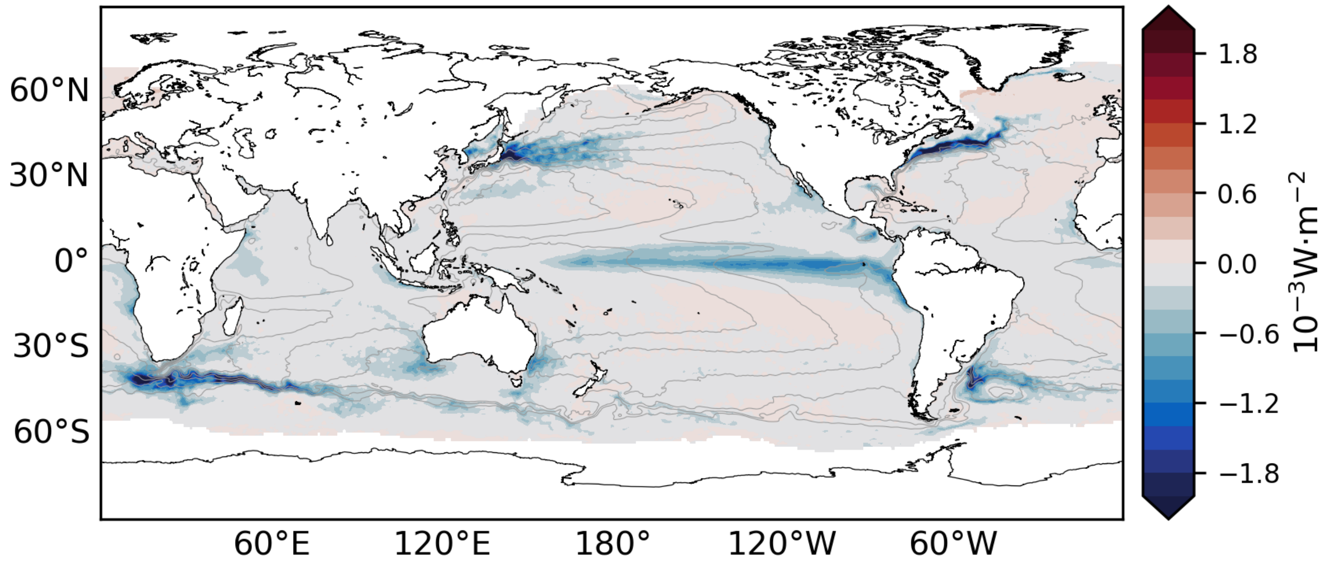

Based on NOAA OISST and JOFURO3 NHF from 1993-2013. (Adapted from Bishop et al. 2020)

- Mesoscale air-sea interaction dissipates more than 70% of EPE in the Kuroshio Extension jet. (Ma et al. 2016)
- This effect acts as a 0.1 TW global sink of EPE based on satellite observations. (Bishop et al. 2020)
- Is this an important process in modulating EPE budget in the global ocean?

Diabatic Eddy Potential Energy Budget

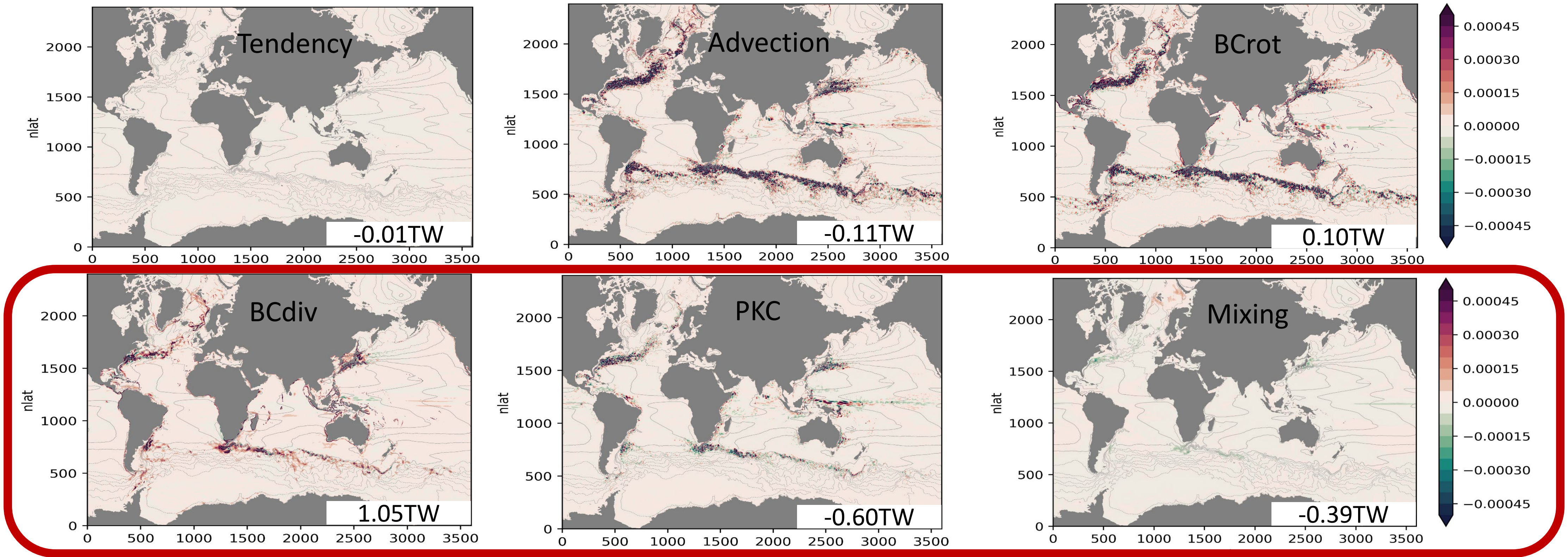

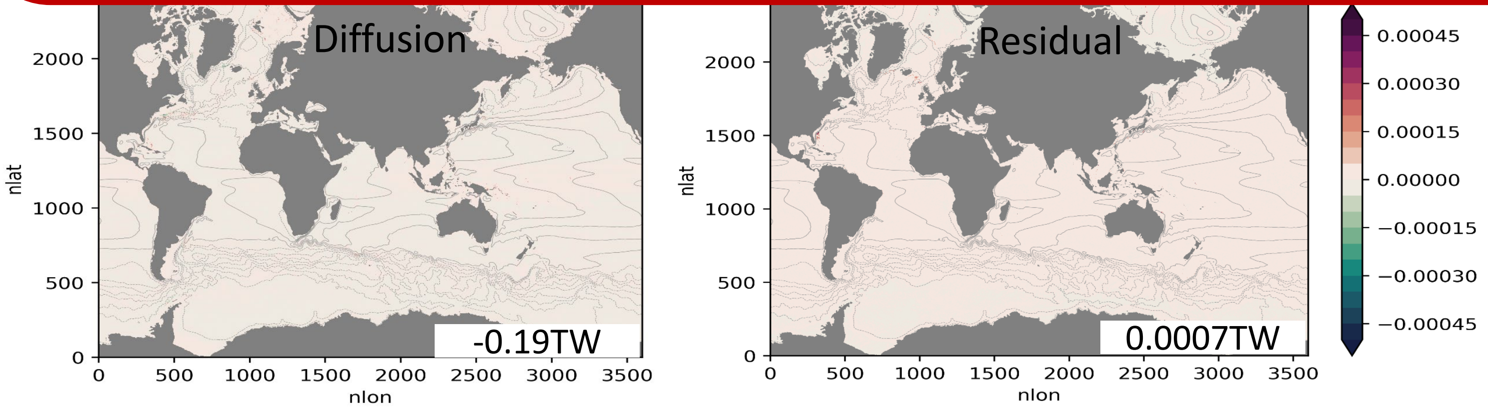

- Maps: vertically integrated T-variance budget terms averaged over 20 years.
- Numbers: global volume integrations.

Note: the residual here is based on the total advection term without partitions. Considering all different dynamic terms separately, the residual is o(-0.03TW).

From 1/10° POP model

Diabatic Eddy Potential Energy Budget

- The rotational BC qualitatively balances the advection of EPE.

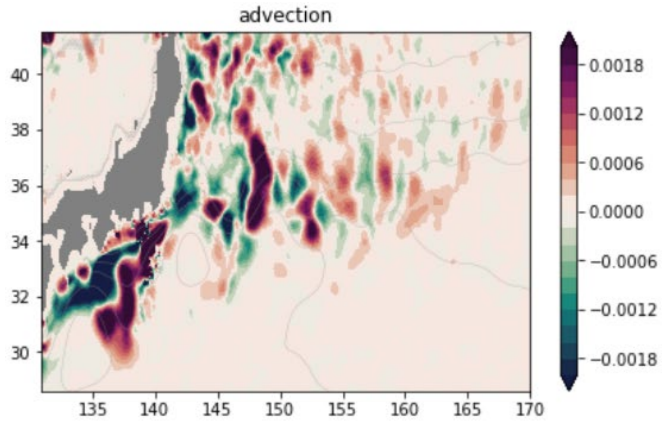

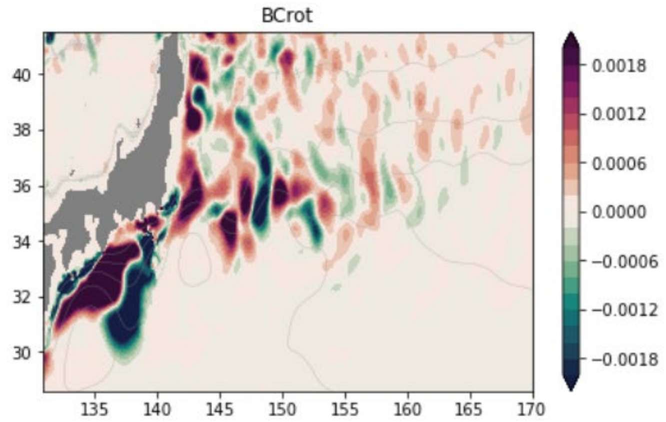

- Diabatic processes play a role in the upper ocean.

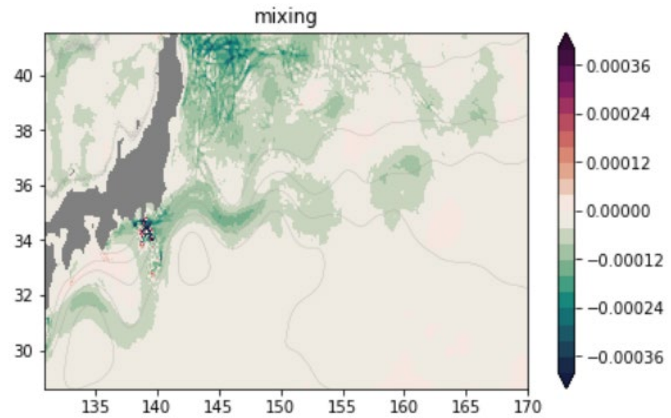

- Spatial distribution of divergent BC aligns with that in the PKC.

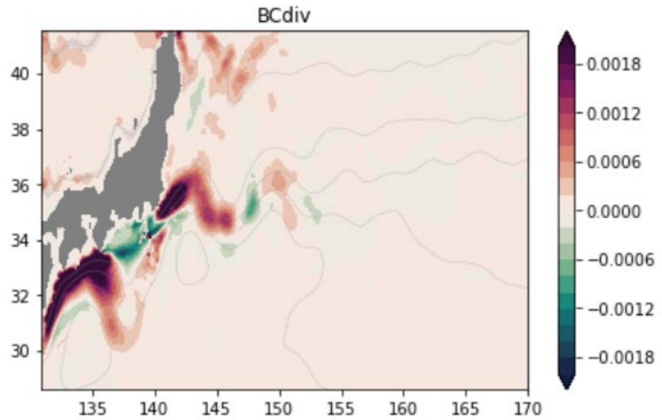

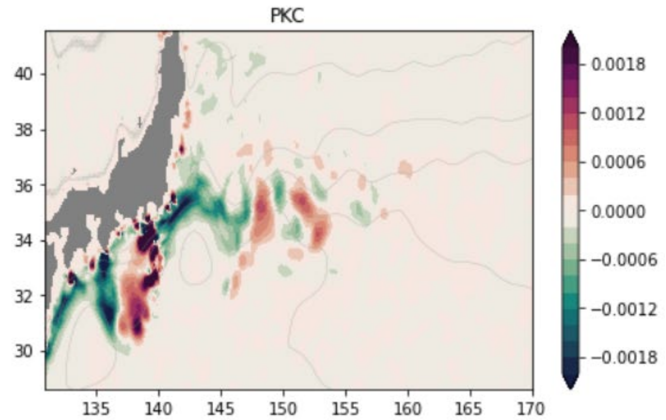

Vertically integrated T-variance budget terms averaged within 20 years based on 1/10° POP.

Diabatic Eddy Potential Energy Budget

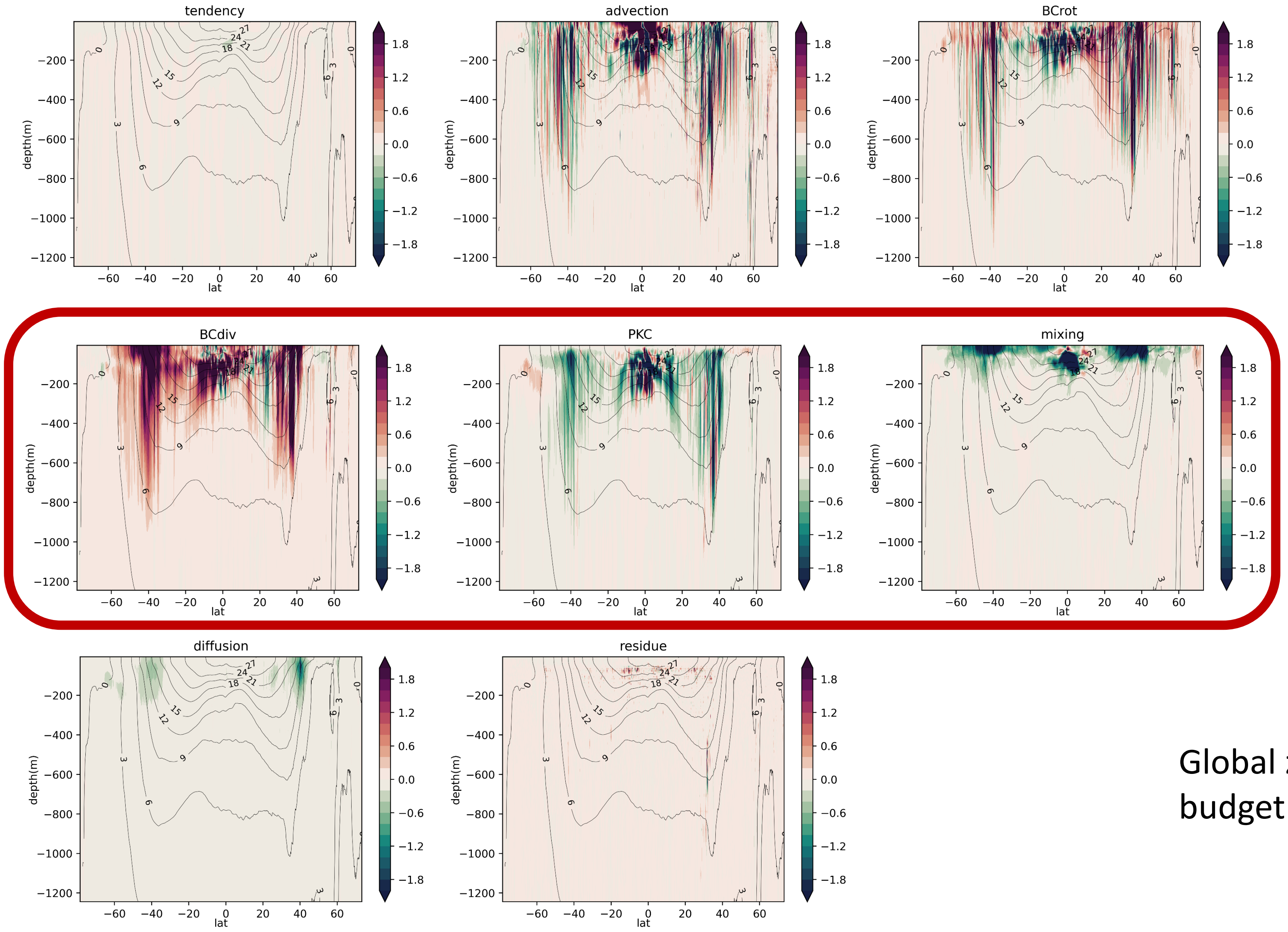

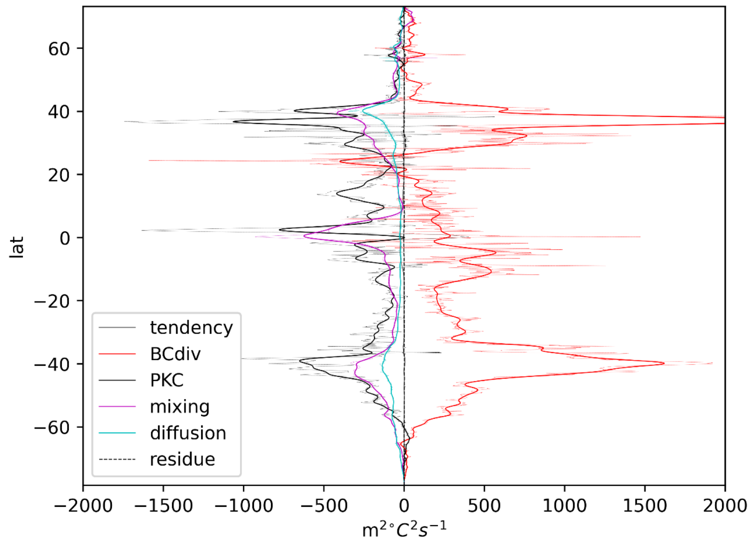

Global zonally and vertically integrated T-variance budget terms based on 1/10° POP in a 20-year period.

Conclusions

- Helmholtz decomposition was applied on the globe to extract the dynamically important eddy heat transport and its related energy conversions in the baroclinic instability.

- The global EPE budget diagnosis was performed in a high-resolution ocean model. It is shown that the conversion from MPE to EKE is not 100% efficient within the baroclinic instability.

- Diabatic processes can destruct ~40% of EPE that would typically be available for conversion to EKE. The mesoscale air-sea interaction accounts for no more than 10% of EPE sink globally.

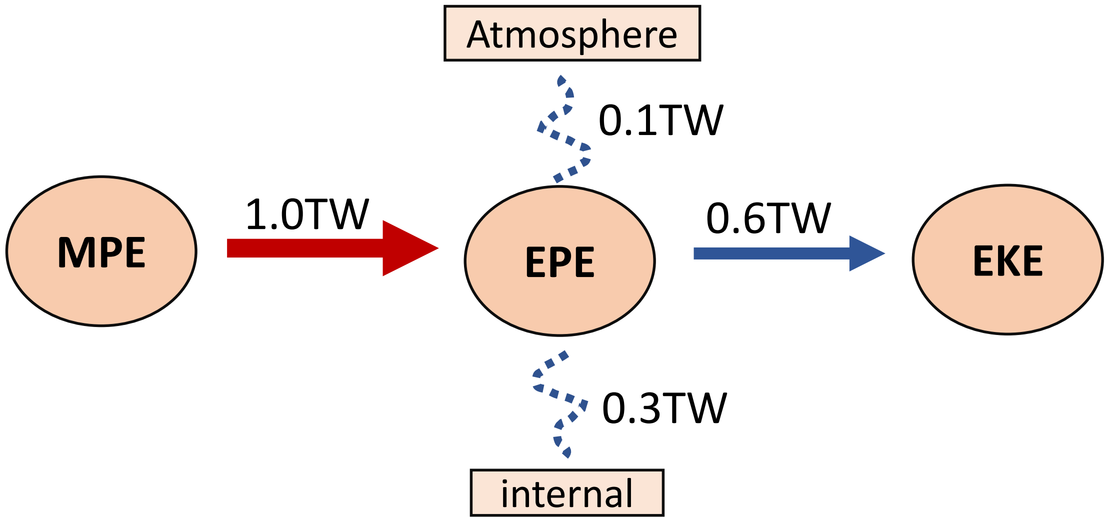

"With full OME-A feedback, CRCM CTRL reveals that nearly 74% of the EPE extracted from MAPE is lost owing to EPE dissipation and less than 22% is converted to EKE…"in the Kuroshio Extension jet.

(Ma et al., 2016 Nature)

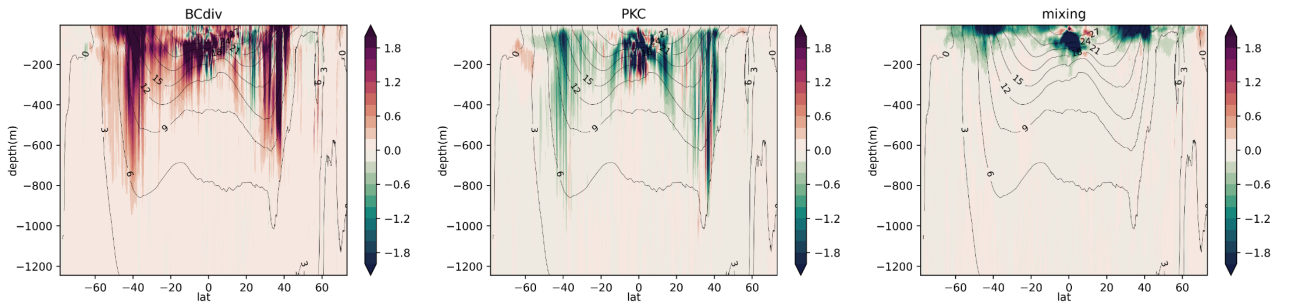

Thank you!

yguo20@ncsu.edu

Diabatic Eddy Potential Energy Budget

Full EPE equation (from thermal contribution):

$$\frac{\partial \frac{\overline{T'^2}}{2}}{\partial t} = -(\overline{\boldsymbol{v}} + \boldsymbol{v}') \cdot \nabla \frac{\overline{T'^2}}{2} - \overline{\boldsymbol{v}'T'} \cdot \nabla_h \overline{T} - \overline{w'T'} \frac{\partial \overline{T}}{\partial z} + T' \frac{\partial}{\partial z}\left(\frac{Q'}{\rho_o C_p} + \kappa \frac{\partial T}{\partial z}\right) + T' \cdot A_h \nabla^2 T$$

- Tendency
- Mean+eddy advection
- BC (BC^{rot}+ BC^{div})
- PKC
- Vertical mixing
- Horizontal diffusion

Notes on closing the budget

Heat equation: $\frac{\partial T}{\partial t} = -\nabla \cdot \boldsymbol{v}T + \frac{\partial}{\partial z}\left(\frac{Q}{\rho_o C_p} + \kappa \frac{\partial T}{\partial z}\right) + A_h \nabla^2 T$

Multiply by T': $T' \frac{\partial T}{\partial t} = -T'\nabla \cdot \boldsymbol{v}T + T' \frac{\partial}{\partial z}\left(\frac{Q}{\rho_o C_p} + \kappa \frac{\partial T}{\partial z}\right) + T' A_h \nabla^2 T$

$$-T'\nabla \cdot \boldsymbol{v}T = -(T'\nabla \cdot \boldsymbol{v}'\overline{T} + T'\nabla \cdot \boldsymbol{v}'T' + T'\nabla \cdot \overline{\boldsymbol{v}}T' + T'\nabla \cdot \overline{\boldsymbol{v}}\overline{T})$$

$$-T'\nabla \cdot \boldsymbol{v}T = \underbrace{-(T'\nabla_h \cdot \boldsymbol{v}T - T'\nabla_h \cdot \boldsymbol{v}T')}_{\text{BC}} \underbrace{- \left(T' \frac{\partial wT}{\partial z} - T' \frac{\partial wT'}{\partial z}\right)}_{\text{PKC}} \underbrace{- T'\nabla \cdot \boldsymbol{v}T'}_{\text{Advection}}$$

Spatial scales in the energy conversions

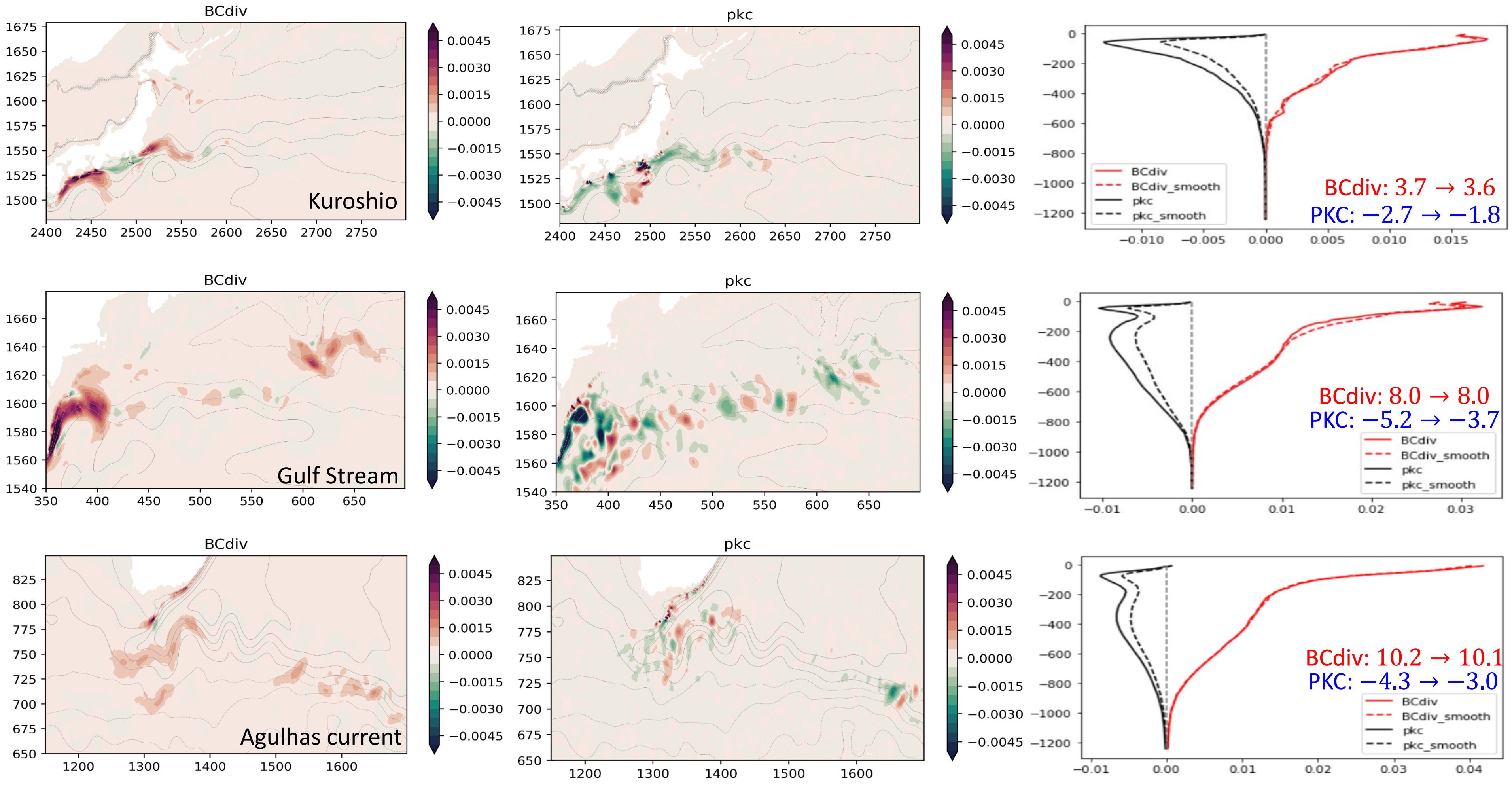

The vertical eddy heat flux is largely influenced by ‘small mesoscale’ processes at less than 50 km, but the baroclinic conversion is virtually unchanged.

Contour maps: vertically integrated divergent BC rate(first column) and PKC rate(second column);
Vertical plots: vertical structures of regional sum of BCdiv (red solid lines) and PKC (black solid lines). The corresponding conversion rates estimated from smoothed fields(convolution filtering with ~50km) are shown with dashed lines.

Seasonality of vertical eddy heat flux

Strong seasonal signal is observed in the vertical eddy fluxes in upper 200m.

$\overline{w'\theta'}^{JAS} / \overline{w'\theta'}^{JFM}$

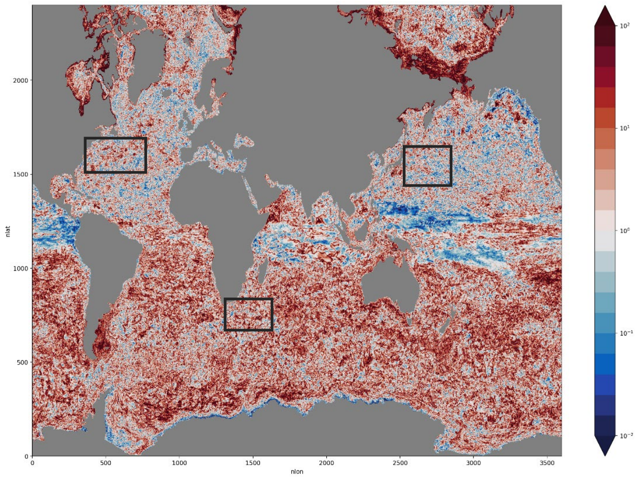

PKC^{JAS} / PKC^{JFM}

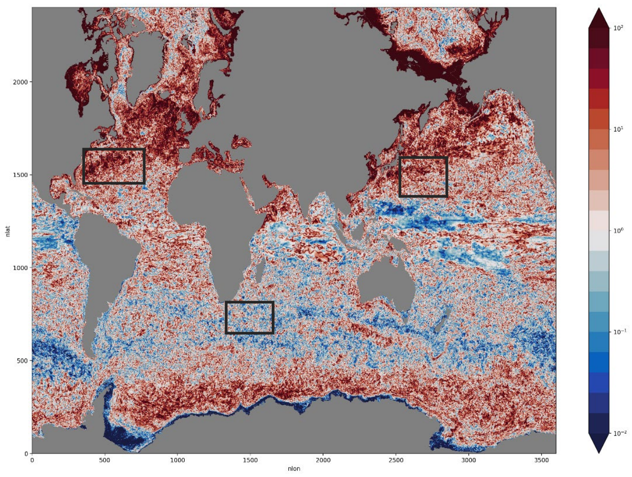

Strong seasonality is observed in the vertical eddy heat flux. The associated energy conversion is significantly modulated by the large-scale mean vertical temperature gradient

Kuroshio

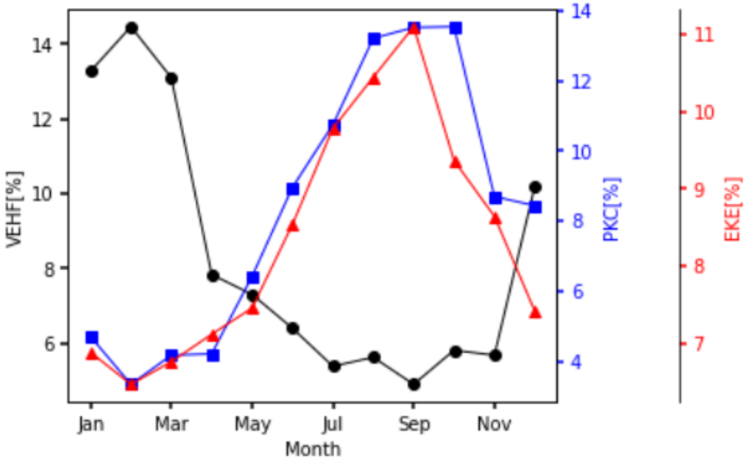

Gulf Stream

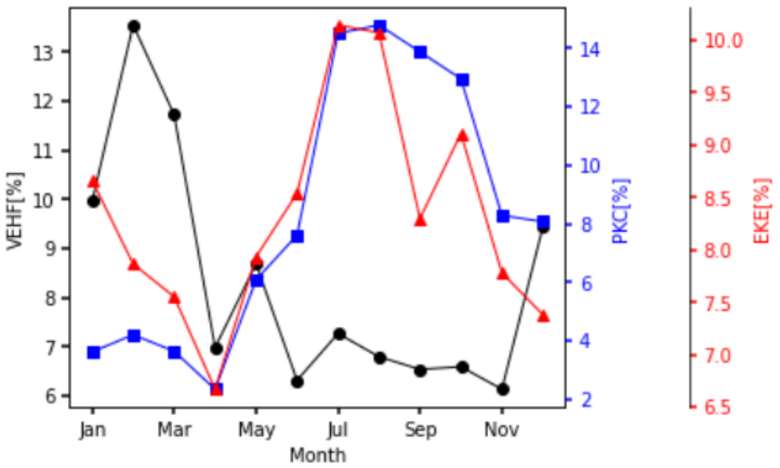

Agulhas

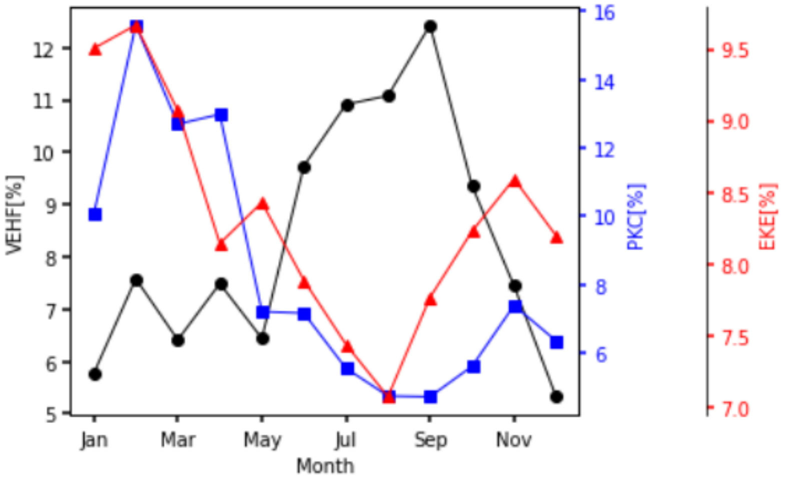

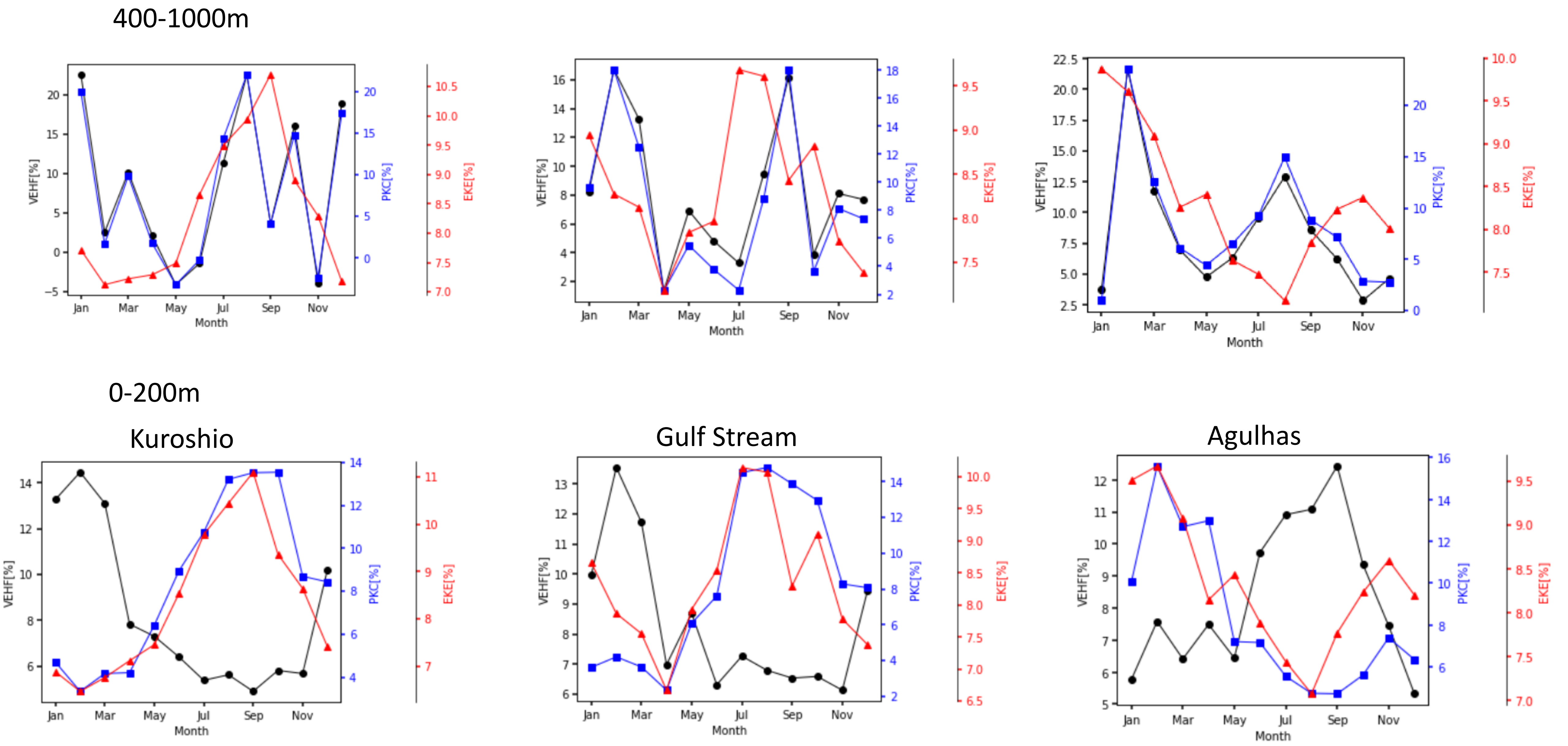
400-1000m
0-200m
Kuroshio
Gulf Stream
Agulhas
VEHF[%]
PKC[%]
EKE[%]
Month
Jan
Mar
May
Jul
Sep
Nov